

# Non-reciprocity in magnon mediated charge-spin-orbital current interconversion

J. Omar Ledesma-Martin,<sup>†</sup> Edgar Galindez-Ruales,<sup>†</sup> Sachin Krishnia,<sup>\*,†</sup> Felix Fuhrmann,<sup>†</sup> Duc Minh Tran,<sup>†</sup> Rahul Gupta,<sup>†</sup> Marcel Gasser,<sup>†</sup> Dongwook Go,<sup>†,‡</sup> Gerhard Jakob,<sup>†</sup> Yuriy Mokrousov,<sup>†,‡</sup> and Mathias Kläui<sup>\*,†,¶,§</sup>

<sup>†</sup>*Institute of Physics, Johannes Gutenberg University Mainz, 55099 Mainz, Germany*

<sup>‡</sup>*Peter Grünberg Institut and Institute for Advanced Simulation, Forschungszentrum Jülich and JARA, 52425 Jülich, Germany*

<sup>¶</sup>*Graduate School of Excellence Materials Science in Mainz, 55099, Mainz, Germany*

<sup>§</sup>*Department of Physics, Center for Quantum Spintronics, Norwegian University of Science and Technology, 7491, Trondheim, Norway.*

E-mail: krishnia@uni-mainz.de; klaeui@uni-mainz.de

## Abstract

In magnetic systems, angular momentum is carried by the spin and orbital degrees of freedom. Non-local devices can be used to study angular momentum transport. They consist of parallel heavy-metal nanowires placed on top of magnetic insulators like yttrium iron garnet (YIG), facilitating the transmission of information by magnons, generated by the accumulation of spin at the interface, created via the Spin Hall Effect (SHE) and detected via the inverse SHE (iSHE). It has been demonstrated that these processes have comparable efficiencies when the role of the detector and injector is reversed, which points to reciprocity of the processes. However, we show that by adding Ru as a source of direct and inverse orbital Hall effect (OHE), the system no longer

exhibits this reciprocity. Specifically, the generation of magnons via the combination of SHE and OHE and detection via the iSHE is found to be about 35% more efficient than the inverse process for our system.

Spin current generation/detection mechanisms and spin transport in magnetic systems have been the topic of intense research interest in the last decade for potential application in spintronic devices as well as for the fundamental understanding of these mechanisms.<sup>1,2</sup> Two main mechanisms, the spin Hall effect (SHE) in the bulk of the heavy metal<sup>3-6</sup> and the Rashba-Edelstein effect (REE)<sup>7-9</sup> at inversion asymmetric interfaces involving high spin-orbit interactions, have been intensively investigated to generate spin currents and a non-equilibrium spin density from a charge current. The spin current and spin accumulation may diffuse and exert a spin-orbit torque on an adjacent magnetic layer.<sup>2,4,6,10,11</sup> The reciprocal process is the generation of spin currents by precessional dynamics of magnetization, which then subsequently diffuses into an adjacent heavy-metal layer and can be detected in terms of a voltage generated through the inverse SHE (iSHE) and/or the inverse REE (iREE) effects.<sup>12-15</sup> Notably, the efficiencies of direct (charge to spin conversion by SHE and REE) and inverse (spin to charge conversion by iSHE and iREE) conversion of spin current have been reported to be very similar in a wide range of materials. This includes non-local devices, where the microscopic origin of the transfer of spin angular momentum between metals and magnetic layers is quite different depending on the latter being conducting or insulating.<sup>15-17</sup> Compared to metallic ferromagnets, where spin transport involves conduction electrons,<sup>6</sup> the transport in insulating magnets (such as in YIG/Pt structures) requires spin transport through magnon creation and annihilation.<sup>17-20</sup>

Spin current-induced magnon dynamics in insulating magnets interfaced with Pt have been extensively studied in the last decade.<sup>18,20,21</sup> In particular, YIG, a magnetic insulator, is notable for its low magnetic damping<sup>22</sup> and long-distance magnon propagation,<sup>17</sup> making it an ideal medium for magnonic studies. The interaction of YIG with spin currents injected from or into thin Pt nanowires via an exchange mechanism enables the generation and

detection of magnons electrically via non-local measurements, bypassing the need for a charge flow within the insulator. This spin current creates a spin accumulation at the interface with YIG, manipulating its magnetic states through spin angular momentum transfer, allowing for the control of magnon generation and propagation. The inverse process, where magnons from YIG are converted back into electrical signals in Pt via the iSHE, demonstrates the crucial bidirectional conversion capability obeying Onsager reciprocity relations.<sup>17</sup>

Recent experimental studies and theoretical models have revealed that charge currents can also induce non-equilibrium orbital accumulation, thereby generating transverse orbital currents via the orbital Hall and orbital Rashba-Edelstein effects (OHE and OREE),<sup>23–27</sup> in analogy to their spin counterparts. These effects originate from complex orbital textures in momentum space and can be present even without spin-orbit coupling (SOC).<sup>28</sup> Predictions of such phenomena have been extended to materials such as transition metals,<sup>29–33</sup> metal-oxide interfaces,<sup>34,35</sup> and two-dimensional systems.<sup>36–38</sup> The emerging field of orbitronics,<sup>23</sup> is dedicated to the exploration and manipulation of orbital angular momentum, aiming to utilize orbital currents independently or in conjunction with the spin degree of freedom of conduction electrons. This emerging interest has stimulated experimental activities to observe and quantify orbital transport phenomena directly. Additionally, it has been demonstrated that orbital currents can be efficiently converted into spin currents in materials with high spin-orbit coupling, such as heavy metals, allowing for the manipulation of ferromagnets. This phenomena has been termed orbital torques. Moreover, very recent observations of the inverse OREE (iOREE) at interfaces such as  $LaAlO_3/SrTiO_3$ <sup>39</sup> and  $Pt/CuO_x$ <sup>40</sup> have shown that orbital currents can be converted back into charge currents, enhancing the potential of non-local magnon transport devices and broadening their applications. These developments allow for a comparison of the efficiencies of OHE and OREE, as well as iOHE and iOREE, via magnon transport within the same device patterned on top of an insulating magnet.

While the approximate reciprocity of the spin-charge interconversion has been reported,<sup>15</sup>

there are a number of reports that claim large orbital torques can be generated by systems where the reciprocal process of orbital pumping is weak. However, previous reports could not compare the orbital to charge and charge to orbital conversion in identical samples, so it is unclear if the differences are due to sample variation or intrinsic non-reciprocity, so it is necessary to study this in a single device.

In this work, we study the effect of a strong OHE material layer (Ru) on the reciprocity between the generation of magnons via OHE and SHE in a Ru/Pt wire and the detection of magnons via iSHE in the Pt. As well as the reciprocal process, the generation of magnons via the SHE in the Pt wire and the detection of magnons via iOHE and iSHE on the Ru/Pt wire of a non-local device. We ascertain the differences to trace them to the Ru layer where the charge to orbital interconversion occurs.

To examine the reciprocity between magnon generation and detection, we study magnon transport in a non-local geometry, as illustrated in Fig. 1(a). Our device comprises two Pt wires and one Pt/Ru wire, all deposited on a 1.5  $\mu\text{m}$  thick YIG film. YIG is characterized by relatively low damping, thus exhibiting long magnon propagation lengths.<sup>17</sup> Additionally, its electrically insulating nature mitigates electrical shunting effects and simplifies magnon generation complexity associated with spin and/or orbital currents originating from the self-torque mechanism. The YIG thin films were grown by liquid phase epitaxy on GGG substrates and are provided by the commercial supplier Matesy GmbH. We use electron beam lithography to define the device pattern. After defining the metal markers for alignment, we fabricated two parallel wires, each 250 nm wide but with different thicknesses: 7 nm and 13 nm, respectively, in two subsequent lithography processes. We use a Singulus Rotaris DC magnetron sputtering tool for the metal deposition. In the next lithography step, we define a third wire, also 250 nm in width, parallel to the existing two Pt wires with equal spacing. We deposit a Pt(1.5 nm)/Ru(4 nm)/MgO(2 nm)/Ta(2 nm) multilayer stack for orbital current generation and detection. Ru is capable of orbital current generation and detection, and Pt is used to convert the orbital current into spin current via spin-orbit

interaction. The capping MgO/Ta is used to protect Ru from oxidation. Hereafter, we will refer to the Pt(1.5 nm)/Ru(4 nm)/MgO(2 nm)/Ta(2 nm) wire as the "Ru wire". The lengths of the Pt and Ru wires are 50  $\mu\text{m}$ . In the final lithography step, we defined contact pads for electrical measurements and deposited Cr(5 nm)/Au(50 nm) via DC magnetron sputtering. The overall device consists of three parallel and equally spaced wires 50  $\mu\text{m}$  in length and 250 nm wide, with a separation between them ranging from 500 nm to 2  $\mu\text{m}$ . A typical scanning electron microscopy image of a device is shown in Fig. 1(a).

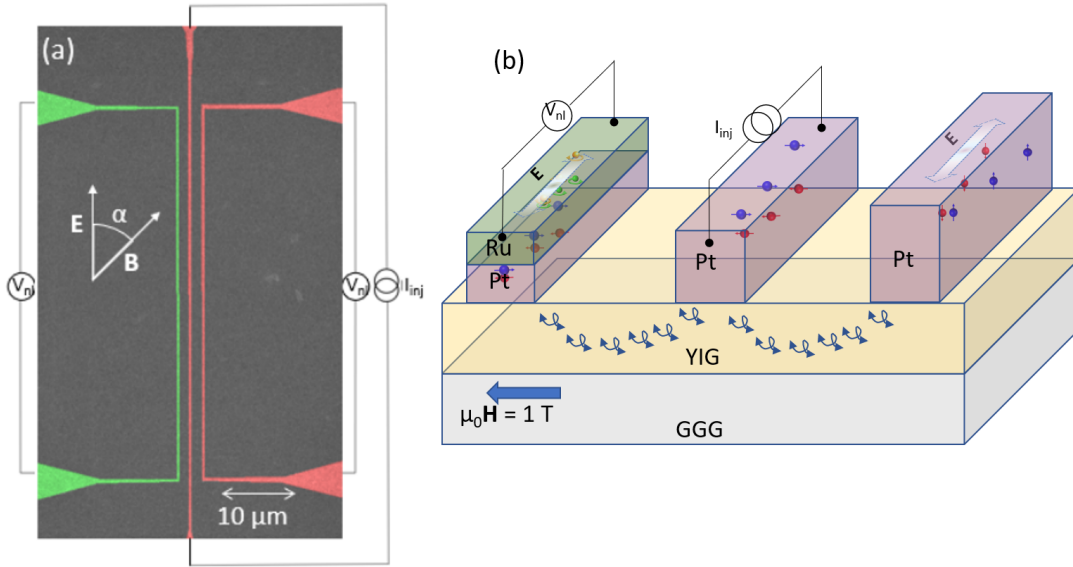


Figure 1: (a) Colored scanning electron microscope (SEM) micrograph of a non-local magnon transport device with the measurement scheme. The device consists of three parallel wires. The two Pt wires having thicknesses of 7 nm and 13 nm (center and right, in red) serve as a source and/or detector of spin current, and the third Pt/Ru wire (left, green) can generate and detect spin and orbital currents. The spacing between the two wires varies from 500 nm to 2  $\mu\text{m}$  in different devices. The angle between the direction of the charge current (parallel to the wire) and the external magnetic field is represented by  $\alpha$ . (b) Schematic representation of the cross-section of a device with the measurement scheme. A spin accumulation is generated by a charge current injection in the middle Pt wire due to the SHE, as shown by red and blue electrons. This spin accumulation generates magnons via spin angular momentum transfer to YIG, which are then converted into spin current and a resultant voltage at the detector Pt (or Ru) wire due to the iSHE (or iSHE + iOHE).

To characterize magnon generation and detection, we conduct non-local electrical measurements. We inject current into one Pt wire (the injector wire), which generates a trans-

verse spin current and a spin accumulation at the YIG/Pt interface, as illustrated in Fig. 1(b). This spin accumulation can couple to the YIG magnetization via the exchange interaction, thereby polarizing magnons within the YIG. These magnons then propagate towards the other Pt electrode (the detector electrode). At the detector electrode, a reciprocal process occurs: the magnons interact with the Pt and are converted into a spin current at the interface, which in turn induces a voltage signal due to the iSHE in Pt. For each measurement, the device is rotated in a fixed magnetic field of 0.1 T. We used a Keithley 6220 as a current source in conjunction with a Keithley 2182A nanovoltmeter in Delta mode, and a constant pseudo-DC current was applied to the injector wire, and the corresponding voltage at the detector wire was measured using a Keithley 2182A nanovoltmeter. The Delta mode measures the voltage for pulses of the same amplitude but opposing polarity, eliminating the thermal offset. We define a non-local resistance ( $R_{nl}$ ) of the detector wire as:

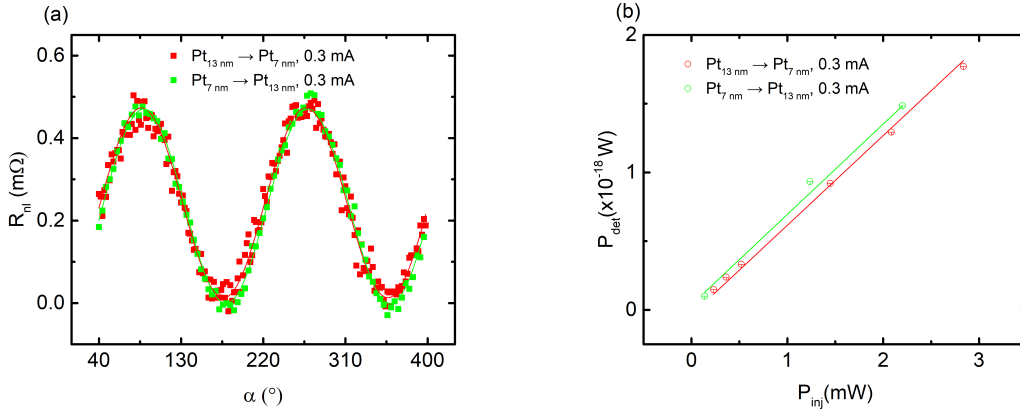


Figure 2: (a) Non-local resistance ( $R_{nl}$ ) as a function of the angle ( $\alpha$ ) between the charge current and the magnetization direction. The red data points correspond to the current injected in the 13 nm thick Pt wire and non-local voltage measurement in the 7 nm thick Pt wire ( $Pt_{13\text{ nm}} \rightarrow Pt_{7\text{ nm}}$ ). Whereas the green points correspond to the current injected in the 7 nm thick Pt wire and non-local voltage measurement in the 13 nm thick Pt wire ( $Pt_{7\text{ nm}} \rightarrow Pt_{13\text{ nm}}$ ). Solid lines represent the sinusoidal fit. An offset baseline has been removed so the non-local resistance values are zero at  $\alpha=0$  degrees. (b) The detected power  $P_{det} = V_{det}^2/R_{det}$  (where  $R_{det}$  is the resistance of the detector wire) as a function of injected power  $P_{inj} = I_{inj}^2 R_{inj}$  (where  $R_{inj}$  is the resistance of the injector wire) for a device with 1  $\mu\text{m}$  spacing between the two wires.

$$R_{nl} = \frac{V_{det}}{I_{inj}}, \quad (1)$$

where  $V_{det}$  is the voltage measured at the detector wire, and  $I_{inj}$  is the current applied to the injector wire. Given the symmetry constraints of the SHE and iSHE mechanisms, the magnon injection/detection process only occurs when there is a component of the spin accumulation that is collinear with the magnetization.<sup>17</sup> Therefore, we measure the dependence of  $R_{nl}$  on the angle between the magnetization and current direction ( $\alpha$ ) by rotating the sample in a fixed in-plane magnetic field of 0.1 T (greater than the anisotropy field of YIG).

In Fig. 2(a), we present the dependence of  $R_{nl}$  as a function of  $\alpha$  for a fixed  $I_{inj} = 0.3$  mA, in a device with a gap of 1  $\mu\text{m}$  between 13 nm and 7 nm thick Pt wires. Note that the current also induces Joule heating, which can generate magnons; however, in this work, we focus only on magnons generated by spin currents by measuring the odd components of voltages for two different current polarities in delta mode. As expected, the  $R_{nl}$  shows a typical sinusoidal dependency on the angle. It shows that the maximum amplitude corresponds to the generation/detection of magnons when the spin polarization and magnetization are collinear to each other and the minimum when they are perpendicular. Next, we verify the reciprocity of magnon transport by interchanging the current and voltage contacts of the injector and detector wires. To make sure that the reciprocity is not only found for nominally, identical wires, we next use Pt wires with different thicknesses and resistances: 13 nm and 7 nm, with resistances of 5  $k\Omega$  and 13  $k\Omega$ , respectively, as injector and detector. This approach also allows us to rule out the possibility that the effect is only observed for certain resistance combinations.

The measured  $R_{nl}$  for the two directions, Pt<sub>7 nm</sub>  $\rightarrow$  Pt<sub>13 nm</sub> (in green) and Pt<sub>13 nm</sub>  $\rightarrow$  Pt<sub>7 nm</sub> (in red), as well as sinusoidal fits for  $R_{nl}$ , is shown in Fig. 2(a). Here, the subscripts 7 nm and 13 nm stand for the thickness of the Pt wires to distinguish them from each other. From the measurement and corresponding fits, we find  $R_{nl}$  (Pt<sub>7 nm</sub>  $\rightarrow$  Pt<sub>13 nm</sub>)  $\approx$

$R_{nl} (Pt_{13\text{ nm}} \rightarrow Pt_{7\text{ nm}}) = 451\ \mu\Omega \pm 5.4\ \mu\Omega$ . As  $R_{nl}$  exhibits similar amplitudes within the error bars in both measurements, we thus conclude that reciprocity is maintained between magnon generation and detection via the SHE and iSHE in our  $Pt \rightarrow Pt$  device.

Additionally, we perform these measurements for several injected currents and compare the injected power with the detected power between the two Pt wires of different resistances. As shown in Fig. 2(b), the detected power increases linearly with the injected power and it exhibits a similar slope ( $6.51 \times 10^{-16} \pm 2.6 \times 10^{-18}$  for  $Pt_{13nm} \rightarrow Pt_{7nm}$  and  $6.57 \times 10^{-16} \pm 4.47 \times 10^{-17}$  for  $Pt_{7nm} \rightarrow Pt_{13nm}$ ) when the injector and detector are interchanged. Based on this observation, we adopt a power-to-power comparison approach hereafter.

Furthermore, the measurements on identical Pt wires (in terms of thickness and resistance) further confirm that magnon generation and detection are reciprocal processes. The data is provided in the supplementary information.

Next, we analyze whether the reciprocity holds for magnon generation/detection when the magnon current is generated via the recently discovered OHE mechanisms. To this end, we replaced one of the 13 nm thick Pt wires with an orbital current generation electrode, i.e., the Ru wire. Note that the spin-charge interconversion processes in the Ru wire exhibit a dominating OHE as demonstrated in our previous work.<sup>30,41</sup> We expect the generation of orbital currents in Ru and its efficient conversion to a spin current in the adjacent 1.5 nm Pt layer. The resulting spin accumulation at the interface with YIG polarizes the magnons, which are detected at the 7 nm Pt detector wire as a voltage generated via the iSHE mechanism, as explained previously. In Fig. 3(a), we show the  $R_{nl}$  dependence as a function of  $\alpha$  for a current  $I_{inj}=0.2$  mA in injector Ru wire (red circle). The  $R_{nl}$  shows the expected angular dependence with an amplitude  $R_{nl} = 2.7\ m\Omega \pm 17\ \mu\Omega$ . Next, we reverse the position of the injector and detector, i.e., we inject the current into the Pt wire, detect the voltage in the Ru wire, and repeat the same measurement, as shown in Fig. 3(a) (blue). The magnons are polarized by the spin accumulations at the YIG/Pt interface and propagate toward the Ru electrode. These magnons accumulate underneath the Ru wire and create a spin current



that flows into the 1.5 nm Pt (below the Ru layer) and is converted into an orbital current. As the thickness of Pt is smaller than the orbital diffusion length, the converted orbital current further diffuses into the Ru layer, where it is converted into a voltage via the inverse OHE. The amplitude of  $R_{nl}$  for magnon injection via pure SHE and detection via iSHE and iOHE is found to be  $R_{nl} = 2.1 \text{ m}\Omega \pm 28 \text{ }\mu\Omega$  for an injected current  $I_{inj} = 0.3 \text{ mA}$  in the Pt electrode. Since the resistance of the detector influences the measured voltage, one should take into account the difference in electrical resistance between the injector and detector when comparing the two processes. To account for this difference between the nanowires ( $R_{Pt} = 12.3 \text{ k}\Omega$  and  $R_{Ru} = 29.3 \text{ k}\Omega$ ), the current is adjusted so that the electrical power applied to both injectors is the same in both cases (1.1 mW). Here, we highlight again that the signal detected at the detector in our experiments solely arises from the magnons polarized by the injector. The voltage signal arising from thermal magnons is not responsible for the measured  $R_{nl}$ . We also emphasize that the magnitude of  $R_{nl}$  differs depending on whether the magnons are generated solely by the SHE in Pt and detected by iOHE and iSHE at the Ru/Pt wire or generated by the OHE and SHE in a Ru/Pt wire and detected via iSHE in Pt.

To better understand the asymmetry in the magnon generation/detection process, we plotted  $P_{det}$  as a function of  $P_{inj}$  for Pt to Ru (red) and Ru to Pt (blue), as shown in Fig. 3(b). The measurements are performed for different distances between the injection and detection wires and for different injected powers  $P_{inj}$  for each measurement; the data is fitted to a sinusoidal function, the value of the amplitude is extracted for each  $P_{inj}$  in each device, and  $P_{det}(P_{inj})$  is fitted to the line  $P_{det}^{fit}(P_{inj})$ . The efficiency from  $P_{inj}$  to  $P_{det}$  is defined as:

$$\xi = \frac{\partial P_{det}^{fit}(P_{inj})}{\partial P_{inj}}. \quad (2)$$

These efficiencies show a clear difference ( $\xi_{Pt \rightarrow Ru} = 1.24 \times 10^{-15} \pm 4.58 \times 10^{-18}$  compared to  $\xi_{Ru \rightarrow Pt} = 1.68 \times 10^{-15} \pm 1.5 \times 10^{-17}$ ), and the respective linear fits can be seen in Fig. 3 (b) for Pt $\rightarrow$ Ru (red) & Ru $\rightarrow$ Pt (blue).

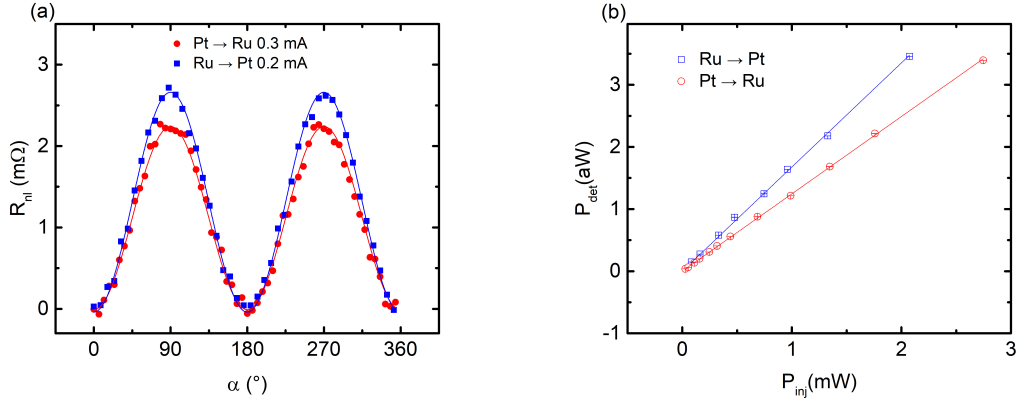


Figure 3: (a) Comparison of the non-local resistance as a function of the angle between the injected current and magnetization direction, when current is injected into Pt (Ru) wire and voltage is detected in Ru (Pt) wire, depicted by red circles (blue squares). The injected current is adjusted to account for differences in the resistance of the two electrodes by maintaining the same injected power at approximately 1.1 mW. (b) Linear fits for power injected ( $P_{inj}$ ) to power detected ( $P_{det}$ ) between wires 800 nm apart for Ru $\rightarrow$ Pt ( $1.68 \times 10^{-15} \pm 1.50 \times 10^{-17}$ ) & Pt $\rightarrow$ Ru ( $1.24 \times 10^{-15} \pm 4.58 \times 10^{-18}$ ). The data for more spacing between the injector and the detector are shown in the supplementary information.

We have demonstrated non-reciprocal generation and detection of magnons in YIG, attributed to the OHE in Ru, by reversing the roles of injector and detector in our experiments. To explain this, we note that a similar non-reciprocity in charge-spin current mutual interconversion has been predicted and experimentally observed in NiFe/CuOx samples due to additional spin current generation via spin vorticity coupling.<sup>42</sup> It is important to note that this effect arises from a substantial resistivity gradient along the thickness of CuOx, leading to a non-uniform spatial distribution in the drift velocity of conduction electrons. This, in turn, induces a vorticity gradient, generating spin current through spin-vorticity coupling;<sup>43,44</sup> however, spin current generation through this mechanism can be ruled out in our device due to the metallic nature of Ru. There are a number of possible microscopic reasons for the observed non-reciprocity. First of all, the Ru-Pt geometry is highly asymmetric and manifestly non-local. The correlation kernel between the perturbation and response at two well-separated points in the system is strongly non-local too, which, in combination with dissipative and non-conserving processes under conditions of broken time-reversal symmetry

by the magnetic field and the magnetization, can result in observed non-reciprocity even in the linear regime.<sup>45</sup> On the microscopic level, the reciprocity of effects observed in Pt wires is based on the reversibility of the magnon generation by spin accumulation and equivalence of the direct and inverse spin-to-charge conversion. In the case of Ru wire, this reversibility can be broken by the presence of the orbital currents and orbital accumulation. In particular, we cannot exclude that a part of the orbital current generated in Ru is able to reach the interface of Pt with YIG, taking part in the generation of magnons. Since we know very little about the principles that govern the transfer of orbital angular momentum of electrons into magnons and its inverse (i.e., generation of orbital angular momentum by magnons), we cannot state with certainty that the two processes are reciprocal, which may be further complicated by the exchange of angular momentum with the spin degree of freedom taking place at the same time. Another source of non-reciprocity may be related to the non-conservation of the orbital current. While in the case of spin, which presents a relatively well-conserved quantity, the reciprocity of direct and inverse SHE effect has been confirmed in various experimental and theoretical studies alike, to date, the same cannot be said about the OHE with certainty, given a strongly non-conserved nature of the orbital current. Finally, the latter may also impact the reciprocity of conversion between the currents of spin and orbital angular momentum.

In conclusion, we have identified non-reciprocal processes in a non-local device with Ru that exhibits a strong OHE. We have found that the reciprocity observed in  $Pt \rightarrow Pt$ , irrespective of the wire thickness and resistance, where SHE and iSHE are means of magnon generation and detection, does not hold once Ru is included. We compare the situation where the magnon generation (detection) involves both OHE and SHE (iOHE and iSHE), first by measuring the change in  $R_{nl}$  while applying the same power in both  $Pt \rightarrow Ru$  and  $Ru \rightarrow Pt$  and then measuring the  $P_{det}$  in the detector while applying different  $P_{inj}$  in the injector and calculating the power to power efficiency in both directions. We obtain a strongly non-reciprocal efficiency  $\xi_{Pt \rightarrow Ru} = 0.73 \xi_{Ru \rightarrow Pt}$ . This strong non-reciprocity is thus

a salient feature when the interconversion of charge and orbital angular momentum occurs.

Note: We note that during the preparation of the manuscript, we became aware of a related work by J.A. Mendoza-Rodarte et al.,<sup>46</sup> which, however, relies on a comparison of the spin injection and the thermal spin generation as two separate effects.

## Acknowledgement

The authors thank the DFG (Spin+X (A01, A11, B02) TRR 173-268565370 and Project No. 358671374), the Horizon 2020 Framework Programme of the European Commission under FETOpen Grant Agreement No. 863155 (s-Nebula); the European Research Council Grant Agreement No. 856538 (3D MAGiC); and the Research Council of Norway through its Centers of Excellence funding scheme, Project No. 262633 "QuSpin". The study also has been supported by the European Horizon Europe Framework Programme under an EC Grant Agreement N°101129641 "OBELIX".

## References

- (1) Hirohata, A.; Yamada, K.; Nakatani, Y.; Prejbeanu, I.-L.; Diény, B.; Pirro, P.; Hillebrands, B. Review on spintronics: Principles and device applications. *Journal of Magnetism and Magnetic Materials* **2020**, *509*, 166711.
- (2) Manchon, A.; Železný, J.; Miron, I. M.; Jungwirth, T.; Sinova, J.; Thiaville, A.; Garello, K.; Gambardella, P. Current-induced spin-orbit torques in ferromagnetic and antiferromagnetic systems. *Rev. Mod. Phys.* **2019**, *91*, 035004.
- (3) Hirsch, J. E. Spin Hall Effect. *Phys. Rev. Lett.* **1999**, *83*, 1834–1837.
- (4) Liu, L.; Lee, O. J.; Gudmundsen, T. J.; Ralph, D. C.; Buhrman, R. A. Current-Induced Switching of Perpendicularly Magnetized Magnetic Layers Using Spin Torque from the Spin Hall Effect. *Phys. Rev. Lett.* **2012**, *109*, 096602.

- (5) Miron, I. M.; Garello, K.; Gaudin, G.; Zermatten, P.-J.; Costache, M. V.; Auffret, S.; Bandiera, S.; Rodmacq, B.; Schuhl, A.; Gambardella, P. Perpendicular switching of a single ferromagnetic layer induced by in-plane current injection. *Nature* **2011**, *476*, 189–193.
- (6) Sinova, J.; Valenzuela, S. O.; Wunderlich, J.; Back, C. H.; Jungwirth, T. Spin Hall effects. *Rev. Mod. Phys.* **2015**, *87*, 1213–1260.
- (7) Manchon, A.; Koo, H. C.; Nitta, J.; Frolov, S. M.; Duine, R. A. New perspectives for Rashba spin-orbit coupling. *Nature Materials* **2015**, *14*, 871–882.
- (8) Bychkov, Y. A.; Rashba, É. I. Properties of a 2D electron gas with lifted spectral degeneracy. *Soviet Journal of Experimental and Theoretical Physics Letters* **1984**, *39*, 78.
- (9) Edelstein, V. Spin polarization of conduction electrons induced by electric current in two-dimensional asymmetric electron systems. *Solid State Communications* **1990**, *73*, 233–235.
- (10) Liu, L.; Pai, C.-F.; Li, Y.; Tseng, H. W.; Ralph, D. C.; Buhrman, R. A. Spin-Torque Switching with the Giant Spin Hall Effect of Tantalum. *Science* **2012**, *336*, 555–558.
- (11) Thiery, N. et al. Nonlinear spin conductance of yttrium iron garnet thin films driven by large spin-orbit torque. *Phys. Rev. B* **2018**, *97*, 060409.
- (12) Rojas Sánchez, J. C.; Vila, L.; Desfonds, G.; Gambarelli, S.; Attané, J. P.; De Teresa, J. M.; Magén, C.; Fert, A. Spin-to-charge conversion using Rashba coupling at the interface between non-magnetic materials. *Nature Communications* **2013**, *4*, 2944.
- (13) Sandweg, C. W.; Kajiwara, Y.; Chumak, A. V.; Serga, A. A.; Vasyuchka, V. I.;

- Jungfleisch, M. B.; Saitoh, E.; Hillebrands, B. Spin Pumping by Parametrically Excited Exchange Magnons. *Phys. Rev. Lett.* **2011**, *106*, 216601.
- (14) Mosendz, O.; Pearson, J. E.; Fradin, F. Y.; Bauer, G. E. W.; Bader, S. D.; Hoffmann, A. Quantifying Spin Hall Angles from Spin Pumping: Experiments and Theory. *Phys. Rev. Lett.* **2010**, *104*, 046601.
- (15) Ciccarelli, C.; Hals, K. M. D.; Irvine, A.; Novak, V.; Tserkovnyak, Y.; Kurebayashi, H.; Brataas, A.; Ferguson, A. Magnonic charge pumping via spin-orbit coupling. *Nature Nanotechnology* **2015**, *10*, 50–54.
- (16) Rojas-Sánchez, J.-C.; Reyren, N.; Laczkowski, P.; Savero, W.; Attané, J.-P.; Deranlot, C.; Jamet, M.; George, J.-M.; Vila, L.; Jaffrès, H. Spin Pumping and Inverse Spin Hall Effect in Platinum The Essential Role of Spin-Memory Loss at Metallic Interfaces. *Phys. Rev. Lett.* **2014**, *112*, 106602.
- (17) Cornelissen, L. J.; Liu, J.; Duine, R. A.; Youssef, J. B.; van Wees, B. J. Long-distance transport of magnon spin information in a magnetic insulator at room temperature. *Nature Physics* **2015**, *11*, 1022–1026.
- (18) Kajiwara, Y.; Harii, K.; Takahashi, S.; Ohe, J.; Uchida, K.; Mizuguchi, M.; Umezawa, H.; Kawai, H.; Ando, K.; Takanashi, K.; Maekawa, S.; Saitoh, E. Transmission of electrical signals by spin-wave interconversion in a magnetic insulator. *Nature* **2010**, *464*, 262–266.
- (19) Wang, H. L.; Du, C. H.; Pu, Y.; Adur, R.; Hammel, P. C.; Yang, F. Y. Scaling of Spin Hall Angle in 3d, 4d, and 5d Metals from  $Y_3Fe_5O_{12}$ /Metal Spin Pumping. *Phys. Rev. Lett.* **2014**, *112*, 197201.
- (20) Lebrun, R.; Ross, A.; Bender, S. A.; Qaiumzadeh, A.; Baldrati, L.; Cramer, J.; Brataas, A.; Duine, R. A.; Kläui, M. Tunable long-distance spin transport in a crystalline antiferromagnetic iron oxide. *Nature* **2018**, *561*, 222–225.

- (21) Collet, M.; de Milly, X.; d’Allivy Kelly, O.; Naletov, V. V.; Bernard, R.; Bortolotti, P.; Ben Youssef, J.; Demidov, V. E.; Demokritov, S. O.; Prieto, J. L.; Muñoz, M.; Cros, V.; Anane, A.; de Loubens, G.; Klein, O. Generation of coherent spin-wave modes in yttrium iron garnet microdiscs by spin-orbit torque. *Nature Communications* **2016**, *7*, 10377.
- (22) Onbasli, M. C.; Kehlberger, A.; Kim, D. H.; Jakob, G.; Kläui, M.; Chumak, A. V.; Hillebrands, B.; Ross, C. A. Pulsed laser deposition of epitaxial yttrium iron garnet films with low Gilbert damping and bulk-like magnetization. *APL Materials* **2014**, *2*, 106102.
- (23) Go, D.; Jo, D.; Lee, H.-W.; Kläui, M.; Mokrousov, Y. Orbitronics: Orbital currents in solids. *Europhysics Letters* **2021**, *135*, 37001.
- (24) Go, D.; Jo, D.; Kim, C.; Lee, H.-W. Intrinsic Spin and Orbital Hall Effects from Orbital Texture. *Phys. Rev. Lett.* **2018**, *121*, 086602.
- (25) Choi, Y.-G.; Jo, D.; Ko, K.-H.; Go, D.; Kim, K.-H.; Park, H. G.; Kim, C.; Min, B.-C.; Choi, G.-M.; Lee, H.-W. Observation of the orbital Hall effect in a light metal Ti. *Nature* **2023**, *619*, 52–56.
- (26) Lyalin, I.; Alikhah, S.; Berritta, M.; Oppeneer, P. M.; Kawakami, R. K. Magneto-Optical Detection of the Orbital Hall Effect in Chromium. *Phys. Rev. Lett.* **2023**, *131*, 156702.
- (27) Ding, S.; Ross, A.; Go, D.; Baldrati, L.; Ren, Z.; Freimuth, F.; Becker, S.; Kammerbauer, F.; Yang, J.; Jakob, G.; Mokrousov, Y.; Kläui, M. Harnessing Orbital-to-Spin Conversion of Interfacial Orbital Currents for Efficient Spin-Orbit Torques. *Phys. Rev. Lett.* **2020**, *125*, 177201.
- (28) Salemi, L.; Berritta, M.; Nandy, A. K.; Oppeneer, P. M. Orbitaly dominated Rashba-

- Edelstein effect in noncentrosymmetric antiferromagnets. *Nature Communications* **2019**, *10*, 5381.
- (29) Krishnia, S.; Sassi, Y.; Ajejas, F.; Sebe, N.; Reyren, N.; Collin, S.; Denneulin, T.; Kovács, A.; Dunin-Borkowski, R. E.; Fert, A.; George, J.-M.; Cros, V.; Jaffrès, H. Large Interfacial Rashba Interaction Generating Strong Spin–Orbit Torques in Atomically Thin Metallic Heterostructures. *Nano Letters* **2023**, *23*, 6785–6791.
- (30) Bose, A.; Kammerbauer, F.; Gupta, R.; Go, D.; Mokrousov, Y.; Jakob, G.; Kläui, M. Detection of long-range orbital-Hall torques. *Phys. Rev. B* **2023**, *107*, 134423.
- (31) Sala, G.; Gambardella, P. Giant orbital Hall effect and orbital-to-spin conversion in *3d*, *5d*, and *4f* metallic heterostructures. *Phys. Rev. Res.* **2022**, *4*, 033037.
- (32) Sala, G.; Wang, H.; Legrand, W.; Gambardella, P. Orbital Hanle Magnetoresistance in a *3d* Transition Metal. *Phys. Rev. Lett.* **2023**, *131*, 156703.
- (33) Lee, S.; Kang, M.-G.; Go, D.; Kim, D.; Kang, J.-H.; Lee, T.; Lee, G.-H.; Kang, J.; Lee, N. J.; Mokrousov, Y.; Kim, S.; Kim, K.-J.; Lee, K.-J.; Park, B.-G. Efficient conversion of orbital Hall current to spin current for spin-orbit torque switching. *Communications Physics* **2021**, *4*, 234.
- (34) Ding, S.; Liang, Z.; Go, D.; Yun, C.; Xue, M.; Liu, Z.; Becker, S.; Yang, W.; Du, H.; Wang, C.; Yang, Y.; Jakob, G.; Kläui, M.; Mokrousov, Y.; Yang, J. Observation of the Orbital Rashba-Edelstein Magnetoresistance. *Phys. Rev. Lett.* **2022**, *128*, 067201.
- (35) Krishnia, S.; Bony, B.; Rongione, E.; Vicente-Arche, L. M.; Denneulin, T.; Pezo, A.; Lu, Y.; Dunin-Borkowski, R. E.; Collin, S.; Fert, A.; George, J.-M.; Reyren, N.; Cros, V.; Jaffrès, H. Quantifying the large contribution from orbital Rashba–Edelstein effect to the effective damping-like torque on magnetization. 2024; <https://doi.org/10.1063/5.0198970>.



- (36) Costa, M.; Focassio, B.; Canonico, L. M.; Cysne, T. P.; Schleder, G. R.; Muniz, R. B.; Fazzio, A.; Rappoport, T. G. Connecting Higher-Order Topology with the Orbital Hall Effect in Monolayers of Transition Metal Dichalcogenides. *Phys. Rev. Lett.* **2023**, *130*, 116204.
- (37) Bhowal, S.; Vignale, G. Orbital Hall effect as an alternative to valley Hall effect in gapped graphene. *Phys. Rev. B* **2021**, *103*, 195309.
- (38) Pezo, A.; García Ovalle, D.; Manchon, A. Orbital Hall physics in two-dimensional Dirac materials. *Phys. Rev. B* **2023**, *108*, 075427.
- (39) El Hamdi, A.; Chauleau, J.-Y.; Boselli, M.; Thibault, C.; Gorini, C.; Smogunov, A.; Barreteau, C.; Gariglio, S.; Triscone, J.-M.; Viret, M. Observation of the orbital inverse Rashba–Edelstein effect. *Nature Physics* **2023**, *19*, 1855–1860.
- (40) Santos, E.; Abrão, J.; Go, D.; de Assis, L.; Mokrousov, Y.; Mendes, J.; Azevedo, A. Inverse Orbital Torque via Spin-Orbital Intertwined States. *Phys. Rev. Appl.* **2023**, *19*, 014069.
- (41) Gupta, R.; Bouard, C.; Kammerbauer, F.; Ledesma-Martin, J. O.; Kononenko, I.; Martin, S.; Jakob, G.; Drouard, M.; Kläui, M. Harnessing Orbital Hall Effect in Spin-Orbit Torque MRAM. 2024.
- (42) Okano, G.; Matsuo, M.; Ohnuma, Y.; Maekawa, S.; Nozaki, Y. Nonreciprocal Spin Current Generation in Surface-Oxidized Copper Films. *Phys. Rev. Lett.* **2019**, *122*, 217701.
- (43) Kobayashi, D.; Yoshikawa, T.; Matsuo, M.; Iguchi, R.; Maekawa, S.; Saitoh, E.; Nozaki, Y. Spin Current Generation Using a Surface Acoustic Wave Generated via Spin-Rotation Coupling. *Phys. Rev. Lett.* **2017**, *119*, 077202.

- (44) Matsuo, M.; Ieda, J.; Harii, K.; Saitoh, E.; Maekawa, S. Mechanical generation of spin current by spin-rotation coupling. *Phys. Rev. B* **2013**, *87*, 180402.
- (45) Tokura, Y.; Nagaosa, N. Nonreciprocal responses from non-centrosymmetric quantum materials. *Nature Communications* **2018**, *9*, 3740, Publisher: Nature Publishing Group.
- (46) Mendoza-Rodarte, J. A.; Cosset-Chéneau, M.; van Wees, B. J.; Guimarães, M. H. D. Efficient Magnon Injection and Detection via the Orbital Rashba Edelstein Effect. 2024.